SIZE DETERMINATION OF *STREPTOCOCCUS MUTANS* 10449 BY LASER LIGHT SCATTERING

V. RYAN, T. R. HART, AND R. SCHILLER, *Department of Physics and Engineering Physics, Stevens Institute of Technology, Hoboken, New Jersey 07030 U.S.A.*

ABSTRACT We have performed three different optical experiments to determine the mean size of the bacterial strain *Streptococcus mutans* 10449, a microorganism with dimensions comparable to the wavelength of the light used in our experiments. The three optical measurements give size values which are consistent with one another and favorably comparable to the consistency we found in identical measurements on a test system of polystyrene spheres of dimensions similar to the bacteria. Homodyne time correlation and power spectrum spectroscopy both depend on the coherence and monochromaticity of laser light for the determination of the mean diffusion coefficient of the scatterers. The Stokes-Einstein equation then relates the diffusion constant to the cell size. Differential light scattering relies for the interpretation of experimental data on the classical theoretical analysis of the angular distribution of scattered light from a scattering object. The three methods yield mean values for the radius of *S. mutans* 10449 of 0.324 ± 0.006 μm, 0.325 ± 0.007 μm, and 0.315 ± 0.009 μm, respectively. However, since intensity correlation spectroscopy provides a direct measure of polydispersity, it would appear to be the preferred single measurement technique for size determination.

INTRODUCTION

Streptococcus mutans is a bacterium under intensive study because of its association with dental caries in experimental animals (1,2) and man (2,3). The nonmotile microorganism forms bacterial aggregates in vitro in the presence of various salivary components. It is believed that a similar process occurs in the oral cavity of host animals and that aggregation is related to the adherence of these bacteria to the enamel surface, followed by the development of plaque, and ultimately, dental caries.

A variety of techniques has been used in the past to study the factors implicated in bacterial aggregation. The laser light scattering methods we have employed permit one to record continuously details of aggregation from the onset of the process to its final stages. However, to determine the absolute rate of aggregate formation it is necessary to set the average size of an individual bacterium accurately. In this study we report on three different optical techniques used to measure the dimensions of the bacterial strain *S. mutans* 10449 and a test system of polystyrene spheres of comparable size.

The use of homodyne light scattering to study the physical characteristics of small particles was first proposed by Pecora in a series of papers in the 1960's (6–8). The theory was applied in experiments to determine the sizes and masses of latex spheres, biological molecules, viruses, etc. Comprehensive reviews appear in Chu (9), French et al. (10), and Berne and Pecora (11).

In this method, light incident on a bacterial suspension is scattered from cells undergoing

Brownian movement. As a result of random cell motions, the incident monochromatic light is Doppler-shifted to a continuous distribution of frequencies. An analysis of the photocurrent power spectrum produced by the scattered light gives the value of the average diffusion constant of the scatterers. In turn, the diffusion constant determines the average cell size through the Stokes-Einstein relation.

If one measures the time autocorrelation function of the homodyne photocurrent, one can make a complementary determination of the average diffusion constant, and hence infer the cell's dimensions. Koppel (12) was the first to show that both the average diffusion constant and the polydispersity of the suspension could be obtained from the experimental data. Carlson (13) and Elson and Webb (14) have reviewed applications of the method to various systems.

Differential light scattering is the traditional technique for determining the sizes of objects with dimensions comparable to the wavelength of light used. A comprehensive review of this method appears in Kerker (4); Wyatt (5) discusses the basic method of measurement and data interpretation for applications in microbiology.

We have measured the intensity of polarized laser light scattered at different angles with respect to the incident beam by a monodisperse solution of *S. mutans* 10449. To determine the bacterial radius we compared our results with theoretical predictions based on classical electromagnetic theory and with the experimental scattering data from polystyrene spheres with dimensions known to be comparable to the bacteria. From the experimental data, we were also able to estimate the polydispersity of the systems.

THEORY

Time Correlation Analysis

The Brownian motion of the suspended particles causes the intensity of scattered light to fluctuate in time and its frequency to be Doppler-shifted. These fluctuations are mirrored in the power output of the photomultiplier tube. We measure directly the time autocorrelation function of the current defined as

$$C(\tau) = \lim_{T\to\infty} \int_{-T}^{T} i(t)i(t+\tau)\,\mathrm{d}t, \tag{1}$$

where $i(t)$ and $i(t+\tau)$ are the current outputs measured at times t and $t+\tau$, respectively. For a dilute polydisperse suspension of noninteracting spherical scatters, $C(\tau)$ is given as (15)

$$C(\tau) = \left[\int_0^\infty A(D)\mathrm{e}^{-K^2D\tau}\,\mathrm{d}D\right]^2. \tag{2}$$

$K = 4\pi\sin(\theta/2)/\lambda$ is the scattering wave vector, with θ the scattering angle and λ the wavelength of light in the suspension medium. $A(D)\mathrm{d}D$ is the intensity of light scattered by all of the suspended particles in the laser beam with diffusion constants between D and $D + \mathrm{d}D$.

To make possible the analysis of Eq. 1, Koppel (12) and Hocker et al. (15) expanded the exponential in the integrand in powers of τ, took the square root of the natural logarithm of $C(\tau)$, and found

$$\ln\,[C(\tau)]^{1/2} = A - B\tau + C\tau^2 + \ldots, \tag{3}$$

where

$$A = \ln \int_0^\infty A(D)\, dD,\ B = \overline{D}K^2 \text{ and } C = \tfrac{1}{2}M_2K^4,$$

while

$$\overline{D} = \int_0^\infty A(D)\, D\, dD / \int_0^\infty A(D)\, dD \tag{4}$$

and

$$M_2 = \int A(D)(D - \overline{D})^2\, dD / \int A(D)\, dD. \tag{5}$$

The data is sufficiently accurate so that B and C may be calculated from the readout on the strip chart recorder. Higher order terms in the expansion of Eq. 3, which would be needed for a more complete description of polydispersity, could not be determined.

From the experimental data and Eq. 3, we can find $\overline{D}$ and a measure of the polydispersity of the system called the fractional average variance of the distribution function (23)

$$f_D^2 = \frac{M_2}{\overline{D}^2} \times 100\%. \tag{6}$$

For spherical scatterers, D is related to the radius R of the suspended particles through the Stokes-Einstein equation,

$$D = kT/6\pi\eta R, \tag{7}$$

with k the Boltzmann constant, T the absolute temperature, and η the viscosity of the suspending fluid. The intensity-average diffusion constant $\overline{D}$ therefore determines an intensity-average scatterer radius $\overline{R}$.

Power Spectrum Analysis

We also can measure directly the power spectrum $S(\omega)$ of the current. $S(\omega)$ is the transform of the time autocorrelation function,

$$S(\omega) = \int_{-\infty}^{\infty} C(\tau)e^{-i\omega\tau}\, d\tau. \tag{8}$$

For polydisperse systems, $S(\omega)$ may be expanded in the moment distributions of the diffusion constant (12),

$$S(\omega) = J \sum_{m=0}^{\infty} \sum_{(m=m_1+m_2)} [(-1)^m/m_1!m_2!]M_{m_1}M_{m_2}Re(2\overline{\Gamma} - i\omega)/(4\overline{\Gamma}^2 + \omega^2]^{m+1}. \tag{9}$$

J is a constant and

$$\left.\begin{aligned} \Gamma &= K^2\overline{D}, \\ M_m &= K^{2m}\int (D - \overline{D})^m A(D)\, dD / \int A(D)\, dD. \end{aligned}\right\} \tag{10}$$

In our experiment, we measured the first term in the expansion of Eq. 9 so that

$$S(\omega) = J\, 2\overline{\Gamma}/4\overline{\Gamma}^2 + \omega^2). \tag{11}$$

$S(\omega)$ of Eq. 11 is a Lorentzian centered at $\omega = 0$, and except for the replacement of the diffusion constant by its average value, it is identical to the single term appearing in the power spectrum for a monodisperse suspension of spherical scatterers. From Eq. 11 and the half-width ($2\bar{\Gamma}$) of the experimental curve for $S(\omega)$, the average diffusion constant $\bar{D}$ of the polydisperse suspension can be determined. With the value of $\bar{D}$ and Eq. 7, one can find the average radius of the suspended particles.

Differential Light Scattering

To determine the average diameter of a suspension of noninteracting scattering objects, the technique known as differential light scattering relies on the classical analysis of light scattered from one of the objects. Mie (16) was the first to find an exact solution to Maxwell's equation for the scattered radiation from an optically homogeneous sphere. Mie's solution may be written

$$J_{\perp}(\theta) = (\lambda^2/4\pi r^2)\,|\sum_{n=1}^{\infty} [A_n P_n^1(\cos\theta)/\sin\theta + B_n(\mathrm{d}P_n^1(\cos\theta)/\mathrm{d}\theta]\,|^2, \tag{12}$$

$$J_{\parallel}(\theta) = (\lambda^2/4\pi r^2)\,|\sum_{n=1}^{\infty} [A_n dP_n^1(\cos\theta)/d\theta + B_n P_n^1(\cos\theta)/\sin\theta]\,|^2, \tag{13}$$

$J_{\perp}$ is the intensity scattered at an angle θ and distance r away from a single sphere when an incident beam of unit intensity is plane-polarized with the electric vector perpendicular to the plane formed by the incident and scattered beams (the plane of observation). $J_{\parallel}$ refers to the corresponding intensity when the electric vector is parallel to the plane of observation. The functions $P_n^1(\cos\theta)$ are the associated Legendre polynomials, while the constants A_n and B_n refer, respectively, to the electric and magnetic multipole coefficients. A_n and B_n are complex functions of spherical Bessel functions which depend on two of the three quantities, m, α, and β where

$$\alpha = (2\pi R/\lambda), \tag{14}$$

and

$$\beta = m\alpha. \tag{15}$$

The parameters above are the refractive index of the sphere relative to the medium, m, the radius of the scattering sphere, R, and the wavelength of light in the medium, λ. With the use of digital computers, Pangonis et al. (17) have tabulated the scattered light intensities $J_{\perp}$ and $J_{\parallel}$ for ranges of the parameters α, m, and λ.

Theoretical predictions of the experiment results must include compensation for geometrical foreshortening. The scattering volume changes as the scattering angle is varied so that Eqs. 12 and 13 must be multiplied by $1/\sin\theta$ before comparison with data.

In differential light scattering, the intensity of scattered light is measured as a function of the scattering angle. The maxima and minima in the resulting pattern can then be matched to sets of theoretical curves generated by computers from Mie's solutions, Eqs. 12 and 13, for scatterers of different radii and different relative indices of refraction. In our case, the relative index of refraction, $m = 1.20$, was known through an independent measurement (18), so that

a choice of the parameter α (or R) of Eq. 14 defined a unique scattering pattern. The size of the particles could then be determined by the angles where extrema appear in the scattering data. With a polydisperse suspension, the extrema in the theoretical analysis remain relatively unshifted in position as long as the average radius in the distribution of bacteria retains the same value as the radius in the monodisperse solution. However, the amplitudes of the extrema are reduced substantially.

This amplitude reduction permits one to estimate the polydispersity in size from the scattering data. We assume that the suspension can be described by a normal distribution $p(R)$ with

$$p(R) = (2\pi)^{-1/2}\,\sigma^{-1}\exp\left[-(R-\overline{R})^2/2\,\sigma^2\right]. \tag{16}$$

Here $\overline{R}$ is the average radius for the suspended particles and σ is the standard deviation about the average. If values for $\overline{R}$ and σ can be found from the experimental data, the sample polydispersity may then be defined by analogy to Eq. 6 as

$$f_R^2 = \frac{\sigma^2}{\overline{R}^2} \times 100\%. \tag{17}$$

This definition of f_R differs from f_D given in Eq. 6. Since f_R is a measure of the dispersion in R and not in D, its significance depends on the validity of the assumption that the size distribution is normal.

We fix $\overline{R}$ by the positions of the extrema in the light scattering data. We then use the distribution, Eq. 16, to find the concentration of scatterers $d\nu$ in a range between R and $R + dR$,

$$d\nu = \nu_0 p(R)\,dR, \tag{18}$$

where ν_0 is the mean concentration for all of the suspended particles. For fixed values of σ in Eq. 16, we use the computer generated numerical solutions to Eq. 12 and Eq. 13 to plot the intensity of scattered light from a polydispersed suspension for the applicable state of polarization,

$$J_\perp^{\text{total}} = \int J_\perp\, p(R)\,dR, \tag{19}$$

or

$$J_\parallel^{\text{total}} = \int J_\parallel\, p(R)\,dR. \tag{20}$$

Finally, in accord with the experimental conditions, we vary the value of σ in either Eq. 19 or Eq. 20 until the best fit is achieved between the theoretical curve and the experimental data, e.g., Fig. 4. With σ determined in this manner, we then can define the polydispersity of the sample through Eq. 17.

MATERIALS AND METHODS

Stock cultures of *S. mutans* 10449 were obtained from the School of Dental and Oral Surgery, Columbia University, New York. Tryptic soy broth (BBL, Cockeysville, Md.) was used exclusively for the growth medium. To create near anaerobic growth conditions, cultures were grown to stationary phase at 37°C without shaking in flasks with tight fitting screw caps.

The phosphate buffer saline used for suspension (Beckman Instruments, Inc., Fullerton, Calif.) has a pH of 7.2. To reduce the amount of dust present in the sample, the buffer was continuously filtered through a Diatom filter (Vortex, Burton, Mich.) for 2 d after preparation. Just before use, the suspension buffer was filtered twice through 0.2 μm Nuclepore filters (Nuclepore Corporation, Pleasanton, Calif.).

To prepare a sample for study, several aliquots from a stationary phase culture were washed three times, then resuspended in saline using a vortex mixer (Vortex) at one-half of their original volume and allowed to stand for 30 s so that the huge, visible clumps settled to the bottom.

The supernatant was filtered once through a 5.0-μm Nuclepore filter to remove large intractable aggregates, and resuspended using a vortex mixer with a quantity of saline to obtain an optical density of 1.1 at 700 nm in a Turner spectrophotometer (Turner Associates, Palo Alto, Calif.). A ½-ml aliquot from the bacterial suspension was diluted with eleven parts of saline in a scattering cell. The sample was vortex-mixed for 15 s in the scattering cell to disperse aggregates. The suspension was then filtered twice through 1.0-μm Nuclepore filters to remove the remaining aggregates. The filtered suspension was diluted with an equal amount of saline in a scattering cell and was studied within minutes of preparation. The final sample contained 2×10^6 single cocci per milliliter as determined by the pour plate technique. The stability of the suspension during the measurement time was verified by microscopic examination of slides prepared from samples.

The optical cell used for the size determination study was a Witnauer-Scherr vertically cylindrical cuvette with a 3.6-cm i.d., flat entrance and exit windows 1.0 cm wide, and a frosted back side. The light source was a helium-neon laser (Spectra-Physics Inc., Mountain View, Calif.; model 125) with the beam polarized vertically.

A time-correlation laser homodyne system was constructed. Fig. 1 shows a schematic of the light scattering apparatus. This system will be discussed in three parts: optics, electronics, and sample.

The apertures defining the scattering volume were chosen from an analysis of the collected coherence areas. When light from an extended source illuminates a detection surface, a diffraction pattern is produced. A coherence area refers to the area surrounding any given point of the detection surface, such that the signals everywhere within the area are partially spatially coherent with those at the given point (degree of coherence $\delta = 0.5$). For an incoherent light source an estimate of the size of a coherence area is λ^2/Ω, where λ is the wavelength of the radiation and Ω is the solid angle subtended by the source at the detector (19,20). Our experiment was designed to have a large enough signal for easy detection, yet not so large as to collect too many interference zones which could average out their effect.

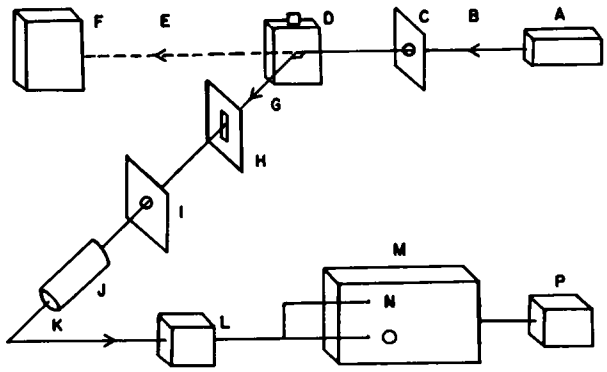

FIGURE 1 Block diagram of scattering apparatus. Data were obtained in a completely darkened room where the only source of light was the laser. Light scattered at a 90° angle from the incident beam was collected and analyzed. A, laser; B, incident laser beam; C, 2.2-mm diam aperture; D, optical cell; E, transmitted laser beam; F, light dump; G, scattered laser beam; H, 1.0-mm wide slit; I, 0.8-mm diam aperture; J, photomultiplier tube; K, photocurrent; L, amplifier; M, multichannel analyzer; N, signal input; O, trigger input; and P, strip chart recorder.

In principle, collection from more than one coherence area should not improve the signal-to-noise ratio. The signal from a single coherent area is directly proportional to the square of the time average photocurrent i_0^2, while the noise is proportional to the current i_0. If the light is collected from N uncorrelated coherence areas, the signal increases to Ni_0^2, but the noise also increases to Ni_0. Hence if the areas were randomly phased with respect to one another, the signal-to-noise ratio should not increase. However, when we actually varied the collection aperture size to intercept larger coherence areas, we observed that the signal-to-noise ratio improved. We found the optimum ratio to be when light was collected from approximately eight coherence areas. Jolly and Eisenberg (21) have made a similar experimental observation, and a theoretical description of the optimal coherence area as a function of the experimental parameters has been given by Hughes et al. (22).

The corona of the laser beam was largely eliminated by a 2.2-mm diam aperture mounted 30 cm in front of the scattering cell. The width of the beam constituting the scattering volume was defined by two apertures aligned between the sample and the photomultiplier. A vertical slit 1.0 mm wide was placed next to the scattering cell. The height of the scattering volume was approximately twice the radius of the beam, 1.36 mm. The second aperture, a 0.8-mm diam circle, was mounted on the front of the photomultiplier located 15 cm from the sample. With the scattering volume set by this geometry, the photocathode intercepted approximately eight coherence areas, the optimum number discussed above.

The collection optics illuminated the photomultiplier at a 90° scattering angle. A photomultiplier (Amperex Electronic Corp., Slatersville, R. I.; model XP1002) with an S-20 spectral response was employed.

A multichannel analyzer (Northern Scientific; model 625C) extracted the time correlation function during each run from the amplified photocurrent when the device was triggered by the photopulses. After each triggering event, 512 channels were scanned. Available adjustable parameters were chosen to optimize the instrument's effectiveness in determining the spectral linewidth in accordance with the analyses of Kelly (24) and Jakeman et al. (20). The photocount rate was determined by attaching an independent counter to the detector; the measured photon flux per coherence time was ~1.5. The trigger was adjusted to respond to the leading edge of the photopulses. The trigger threshold was readjusted for each run in response to possible drifts of the average photocount rate. The correlation time per channel per coherence time was ~0.024. The time correlation function appeared in about the first 16 channels, indicating that the number of observed field correlation times was close to 1. The remaining channels were averaged to give an accurate determination of the baseline. Total photon collection time per run was between 30 and 45 s. An average of six runs was taken for each sample studied.

In addition to the biological considerations discussed earlier, sample assembly depended upon several optical factors. The scattering cell did not introduce abberations such as light depolarization or focal distortions. The liquid medium in which the bacteria were suspended did not absorb light strongly. The dust and bacterial debris in the sample were kept at a minimum.

The concentration of bacteria was adjusted to optimize the desired scattering. A lower limit of 10^5 cocci per milliliter was sufficiently large to provide a detectable scattered intensity and insure that occupation-number fluctuations in the scattering volume were insignificant. An upper limit of 10^9 cocci per milliliter was low enough to avoid correlated movement and prevent significant multiple scattering (5).

The power spectrum was measured by feeding the photomultiplier output into a tuned amplifier (Princeton Applied Research Corp., Princeton, N.J.; model 110) for frequency analysis, then into a squarer unit (Princeton Applied Research Corp.; model 230) for rectification. The results were displayed on a strip chart recorder. The tuned amplifier and squarer were used as a spectrum analyzer. Free experimental parameters were adjusted to optimum values to minimize the statistical errors in accordance with the analysis of Degiorgio and Lastovka (25). Our photocounting rate per coherence time was 1.5. Data were obtained with an average frequency bandwidth to half-width at half-height ratio of ~0.1 using a fixed Q (i.e., ratio of center frequency to bandwidth) of 10. An average of 15 frequencies was used. The time constant of the integrator was 3 s. Two runs were taken for each sample studied.

To obtain angular measurements for differential light scattering, the sample holder is fixed in position

and the collection apertures and photomultiplier are mounted to a turntable which surrounds the sample and can be rotated manually. The differential light scattering electronics consist of an electrometer (Keithley Instruments, Inc., Cleveland, Ohio; model 610C) that monitors the photomultiplier voltage output and displays results on a strip chart recorder. The instrument response time was virtually instantaneous and the signal was sufficiently noise-free so that the scattering angle could be smoothly varied from 45° to 130°. The turntable was ruled to within 0.1° accuracy.

RESULTS

Latex Spheres

The three techniques were tested using a saline suspension of 0.6-μm diam polystyrene spheres with a relative index of refraction of 1.20. Both values were determined by the manufacturer, Dow Chemical Company, Midland, Mich. Care was taken to insure that the sample was ultraclean. The concentration of latex particles, about 10^7 particles per milliliter, did not produce significant amounts of multiple scattering, as no halo was visible surrounding the scattering volume. Data in ten independent trials by time correlation analysis of the polystyrene suspension gave an average diameter of 0.611 ± 0.006 μm and a polydispersity f_D of Eq. 6 of 3.0 ± 0.3%. Twelve power spectra of the polystyrene suspension resulted in an average diameter of 0.620 ± 0.006 μm. Results obtained by differential light scattering from the polystyrene suspension in four independent trials showed angular scattering patterns which differed from each other by < 0.1%. The average diameter was 0.606 μm with a polydispersity f_R of Eq. 17 ~ 5%. Hence all three techniques have the potential to reveal accurate information about the dimensions of scatterers.

Time Correlation Data for S. mutans

The photocurrent correlation function obtained for the *S. mutans* suspension is shown for the first 15 channels in Fig. 2. The zero of the time dependent function used for analysis was determined by averaging the correlation function over 10 channels at very large values of τ.

The method of cumulants, summarized in Theory (above), was applied to the data. The resulting coefficients yielded values of $\overline{D} = 8.24 \times 10^{-9}$ cm^2/s and $M_2 = 0.2 \times 10^{-17}$ cm^4/s^2. The value of the second moment, M_2, yielded a polydispersity of 17% from f_D of Eq. 6.

If we combine the errors due to statistical fluctuations and the graphical technique employed for analysis, the expected accuracy is ± 2% for the average diffusion constant and ± 10% for the dispersion about the average diffusion constant:

$$\overline{D} = (8.24 \pm 0.16) \times 10^{-9} \text{ cm}^2/\text{s}$$

$$f_D = 17\% \pm 3\%.$$

The bacterial radius, calculated from the above data and the Stokes-Einstein relation, was found to be 0.315 ± 0.009 μm.

Power Spectrum Data for S. mutans

Power spectrum data were obtained for the *S. mutans* suspension as a function of frequency using the spectrum analyzer. Since in all measurements the Q (frequency divided by bandwidth) of the tuned amplifier was held constant, the conventional homodyne power spectrum shown in Fig. 3 was secured by dividing each data point by its corresponding frequency.

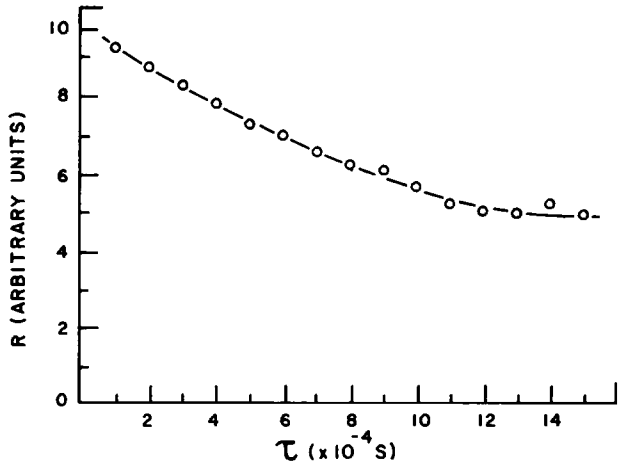

FIGURE 2 Time correlation function $R(\tau)$ vs. time for size determination. The time correlation function is given in arbitrary units, since the amplitude is nonessential to the size determination. Total photon collection time was 45 s. Each data point corresponds to a different channel in the multichannel analyzer, and the dwell correlation time τ per channel is equal to 1×10^{-4} s. The uncertainty in the value of R for each data point is indicated by the diameter of the open circles. The solid line is simply a guide for the eye.

The power spectrum was fitted to a single Lorentzian curve using a least squares analysis. The resulting half-width of 100.8 Hz fit with a root-mean-square deviation of 2%, and when the measured diffusion constant was used in the Stokes-Einstein relation, the radius of an *S. mutans* bacterium was determined to be 0.325 ± 0.007 μm.

Differential Light Scattering Data for S. mutans

Fig. 4 shows the differential light scattering pattern obtained for the *S. mutans* suspension when the scattering angle is measured from the forward direction. Two minima and one

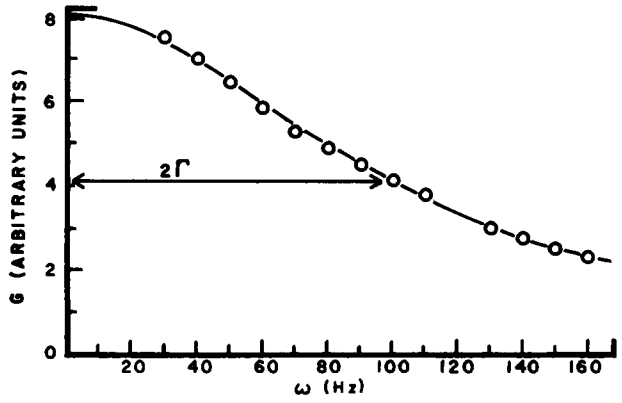

FIGURE 3 Power spectrum $G(\omega)$ vs. frequency shift ω for size determination. The power spectrum is given in arbitrary units, since the amplitude is nonessential to the size determination. Photon collection time per frequency was 1 min and values presented were averaged over that time period. The uncertainty in the value of G for each data point is indicated by the diameter of the open circles. The best fit single Lorentzian curve (Eq. 11) is also shown.

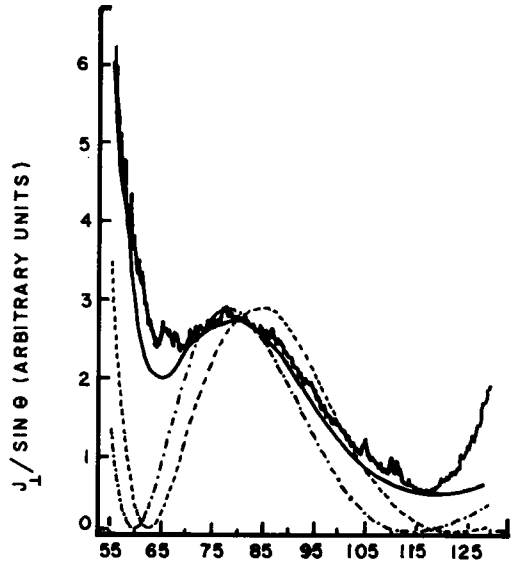

FIGURE 4 Differential light scattering pattern data for size determination. The intensity of scattered light collected at a given angle is equal to the product of the intensity $J_\perp$ scattered at that angle from a single sphere times the number of scatterers contained in the scattering volume which is proportional to sin θ. The scattered intensity is given in arbitrary units, since the amplitude is nonessential to the size determination. The angle θ is measured from the direction of the incident beam. Some of the lack of smoothness in the data is due to manual rotation of the turntable. (- - -) Values calculated for $R = 0.316$ μm and $m = 1.05$; (- · -) values calculated for $R = 0.331$ μm and $m = 1.05$; and (———) values calculated for mean radius of 0.324 μm. $m = 1.05$, and polydispersity of 13%, where R is the radius of a single spherical scatterer and m is the relative index of refraction. All theoretical curves were based on tables by Pangonis et al. (17) and were corrected for geometrical foreshortening.

maximum occur over the angular range studied. Also shown in Fig. 4 are curves predicted by the Mie theory of scattering from a homogeneous sphere and computed by Pangonis et al. (17) for a relative index of refraction m of 1.05 (18) and size parameter α values of 4.2 and 4.4. These curves, which include compensation for geometrical foreshortening, correspond to scatterers of radii 0.316 and 0.331 μm, respectively. They were selected from the tabulated curves of reference 17 as best fits to the observed angular scattering pattern using the criterion of minimum root-mean-square deviation of angles at which extrema occur.

If we assume that the polydispersity can be described by a normal distribution about the best fit mean radius of 0.324 ± 0.006 μm, a series of theoretical curves can be generated for polydispersities of 5, 8, 10, 13, 15, 18, and 20% and compared with the experimental angular scattering results. The normal distribution of cells having 15% polydispersity in size is shown in Fig. 5. As shown in Fig. 4, this curve fits the data best with a root-mean-square deviation of $< 2\%$.

The differences between the 13% polydisperse theory curve and the data are accounted for by optical and other experimental artifacts. For example, we observed that an increase in the concentration of bacteria filled in the small angle minimum in the experimental curves. Thus, multiple scattering could account for the higher scattered intensity at the first minimum. A back-reflected component of the incident beam from the exit window of the scattering cell

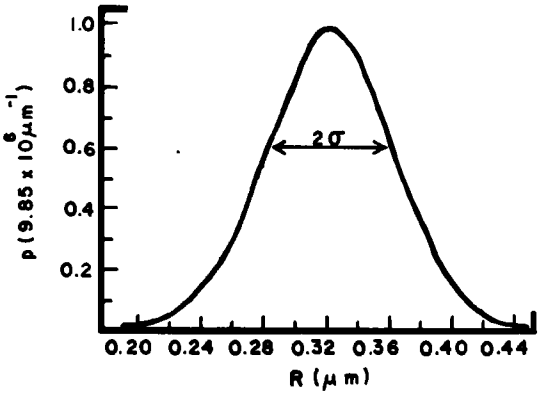

FIGURE 5 Normal distribution function $p(R)$ for radii R of bacteria. The curve was calculated from Eq. 16 with $R = 0.324$ μm and a polydispersity of 13% ($\sigma = 0.0405$ μm). The full width of the distribution at $e^{-1}\,p(R)$ is 2σ. $p(0.324\ \mu m) = 9.85 \times 10^6\ \mu m^{-1/2}$.

passes through the sample. This back-reflected beam has the effect of mirror-imaging the scattering pattern about 90° and manifests itself as a sharp rise in the data at scattering angles $> 120°$.

The curves are more sensitive to average size variations than to polydispersity changes. The size determination is accurate to within 3%. A change of 5% in polydispersity would produce little noticeable effect on the accuracy of the size measurement.

CONCLUSION

The three techniques described for the measurement of the average size of the strain studied gave results which differed from each other within the expected accuracies of the experiments. In addition, it was possible to determine the degree of polydispersity directly from the autocorrelation function and after considerable calculation from the angular scattering pattern. By averaging the measured values, the average radius of an *S. mutans* 10449 bacterium was determined to be 0.321 ± 0.007 μm with a polydispersity between 13 and 17%. Intensity correlation spectroscopy would appear to be the preferred single measurement technique for size determination.

This investigation was supported in part by U.S. Public Health Service grant 5 ROI DE04559 from the National Institute of Dental Research. This article contains, *inter alia*, the results of a doctoral dissertation submitted by Dr. Ryan to the Graduate School of Stevens Institute of Technology.

Received for publication 26 March 1980.

REFERENCES

1. FITZGERALD, R. J. 1968. Dental caries research in gnotobiotic animals. *Caries Res.* **2**:139.
2. BOWEN, W. H. 1969. The induction of rampant dental caries in monkeys *(Macaca iris)*. *Caries Res.* **3**:227.
3. KRASSE, B., H. V. JORDAN, S. EDWARDSSON, I. SVENSON, and L. TRELL. 1968. The occurrence of certain "caries-inducing" streptococci in human dental plaque material. *Arch. Oral Biol.* **13**:911.
4. KERKER, M. 1979. The Scattering of Light and other Electro-magnetic Radiation. Academic Press, Inc., New York. 183–263.
5. WYATT, P. J. 1974. Methods in Microbiology. Vol. 8. Academic Press, Inc., New York.

6. PECORA, R. 1964. Doppler shifts in light scattering from pure liquids and polymer solutions. *J. Chem. Phys.* **40**:1604.
7. PECORA, R. 1965. Doppler shifts in light scattering. II. Flexible polymer molecules. *J. Chem. Phys.* **43**:1562.
8. PECORA, R. 1968. Spectrum of light scattered from optically anisotropic macromolecules. *J. Chem. Phys.* **49**:1036.
9. CHU B. 1974. Laser Light Scattering. Academic Press, Inc., New York. 317.
10. FRENCH, M. J., J. C. ANGUS, and A. G. WALTON. 1969. Laser beat frequency spectroscopy. *Science (Wash. D.C.).* **163**:145.
11. BERNE, B. J., and R. PECORA. 1976. Dynamic Light Scattering. John Wiley and Sons, Inc., New York. 376.
12. KOPPEL, D. E. 1972. Analysis of macromolecular polydispersity in intensity correlation spectroscopy: the method of cumulants. *J. Chem. Phys.* **57**:4814.
13. CARLSON, F. D. 1975. The application of intensity fluctuation spectroscopy to molecular biology. *Annu. Rev. Biophys. Bioeng.* **4**:273.
14. ELSON, E. L., and W. W. WEBB. 1975. Concentration correlation spectroscopy: a new biophysical probe based on occupation number fluctuation. *Annu. Rev. Biophys. Bioeng.* **4**:311.
15. HOCKER, L., J. KRUPP, G. B. BENEDEK, and J. VOURNAKIS. 1973. Observations of self-aggregation and dissociation of *E. coli* Ribosomes by optical mixing spectroscopy. *Biopolymers.* **12**:1677.
16. MIE, G. 1908. *Ann. Phys. (Leipzig).* **25**:377. Quoted in J. A. Stratton, 1941. Electromagnetic Theory. McGraw-Hill Book Co., Inc., New York. Chapter 9.
17. PANGONIS, W. J., and W. HELLER. 1960. Angular Scattering Functions for Spherical Particles. Wayne State University Press, Detroit. 222.
18. WYATT, P. J. 1970. Cell wall thickness, size distribution, refractive index ratio and dry weight content of living bacteria *(Staphylococcus aureus). Nature (Lond.).* **226**:277.
19. CUMMINS, H. Z., and H. L. SWINNEY. 1970. Light beating spectroscopy. *Prog. Opt.* **8**:133.
20. JAKEMAN, E., C. J. OLIVER, and E. R. PIKE. 1970. Effects of spatial coherence on intensity fluctuation distributions of Gaussian light. *J. Phys. A. Gen. Phys.* **3**:L45.
21. JOLLY, D., and H. EISENBERG. 1976. Photon correlation spectroscopy, total intensity light scattering with laser radiation, and hydrodynamic studies of a well fractionated DNA sample. *Biopolymers.* **15**:61.
22. HUGHES, A. J., E. JAKEMAN, C. J. OLIVER, and E. R. PIKE. 1973. Photon correlation spectroscopy. Dependence of linewidth error on normalization, clip level, detector area, sample time and count rate. *J. Phys. A. Gen. Phys.* **6**:1327.
23. BEERS, YARDLEY. 1957. Introduction to the Theory of Error. Addison-Wesley Publishing Company, Inc., Reading.
24. KELLY, H. C. 1971. A comparison of the information-gathering capacities of photon-correlation devices. *J. Quantum Electronics.* **7**:541.
25. DEGIORGIO, V., and J. B. LASTOVKA. 1971. Intensity-correlation spectroscopy. *Phys. Rev.* **4**:2033.